NSRRC - J05238 (2016)

JOURNAL OF APPLIED PHYSICS 119, 215308 (2016)

Investigations of rapid thermal annealing induced structural evolution of ZnO: Ge nanocomposite thin films via GISAXS

Abdullah Ceylan,[1,a)] Yusuf Ozcan,[2] Ilghar Orujalipoor,[3] Yen-Chih Huang,[4] U-Ser Jeng,[4] and Semra Ide[1,3]
[1]*Department of Physics Eng., Hacettepe University, Beytepe, 06800 Ankara, Turkey*
[2]*Department of Electricity and Energy, Pamukkale University, Denizli, Turkey*
[3]*Department of Nanotechnology and Nanomedicine, Hacettepe University, Beytepe, 06800 Ankara, Turkey*
[4]*National Synchrotron Radiation Research Center, 101 Hsin-Ann Road, Hsinchu Science Park, Hsinchu, Taiwan*

(Received 4 May 2016; accepted 24 May 2016; published online 7 June 2016)

In this work, we present in depth structural investigations of nanocomposite ZnO: Ge thin films by utilizing a state of the art grazing incidence small angle x-ray spectroscopy (GISAXS) technique. The samples have been deposited by sequential r.f. and d.c. sputtering of ZnO and Ge thin film layers, respectively, on single crystal Si(100) substrates. Transformation of Ge layers into Ge nanoparticles (Ge-np) has been initiated by *ex-situ* rapid thermal annealing of asprepared thin film samples at 600 °C for 30, 60, and 90 s under forming gas atmosphere. A special attention has been paid on the effects of *reactive* and *nonreactive* growth of ZnO layers on the structural evolution of Ge-np. GISAXS analyses have been performed via cylindrical and spherical form factor calculations for different nanostructure types. Variations of the size, shape, and distributions of both ZnO and Ge nanostructures have been determined. It has been realized that GISAXS results are not only remarkably consistent with the electron microscopy observations but also provide additional information on the large scale size and shape distribution of the nanostructured components. *Published by AIP Publishing.* [http://dx.doi.org/10.1063/1.4953352]

I. INTRODUCTION

Quantum confinement of electrons and holes in semiconductors by size reduction below exciton Bohr radius leads to pronounced variations in optical and electrical properties. This fact can be made useful by incorporating quantum confined semiconducting nanostructures in suitable host materials for targeted optoelectronic properties. In recent years, ZnO thin films including nanostructured Germanium nanoparticles (Ge-np) have attracted a considerable attention due to their potential applicability on new opto-electronic devices.[1,2] Ge acquiring a comparatively larger Bohr radius, which is about 24 nm, makes it more attractive as far as the deposition easiness is concerned. In the literature, although there have been several works on Ge doped ZnO thin film structures[3–5] the number of works on Ge nanoparticles embedded in a ZnO matrix is limited.[6–8] We have recently reported the detailed structural investigations of ZnO: Ge nanocomposite thin films prepared by sputtering followed by an *ex-situ* rapid thermal annealing (RTA) process.[9,10] It has been realized that growth conditions of a ZnO host strongly affects the crystal structure of Ge nanoparticles forming after RTA process. The reactive growth of ZnO results in a compact lattice within which Ge nanoparticles would cluster into smaller size by acquiring a simple tetragonal phase known as ST12. In 1965, Bates *et al.* first discovered ST12-Ge upon applying high pressures (>12 GPa) on a diamond cubic-Ge.[11] Theoretical band structure studies revealing ST12-Ge as a direct band semiconductor with 1.47 eV energy gap attracted further attention due to the potential optoelectronics applications.[12] Recent studies have also proved the formation of ST12 phase in Ge-np synthesized by different methods such as laser ablation in liquid media (deionized water or toluene) and reduction of $GeCl_4$.[13–15] Given the application potential of ST12 Ge, it is required to further understand the structural evolution of Ge-np within the ZnO host. In the ZnO: Ge nanocomposite thin films, ZnO and Ge form significantly different nanostructures, i.e., former being c-axis oriented cylindrical and latter being spherical or ellipsoidal, therefore, it is plausible to consider scattering techniques for in depth analyses due to pronounced difference of scattering crossections. That is why, in this study we have chosen to utilize grazing incidence small angle x-ray spectroscopy (GISAXS) technique as it is known to probe nanoscale surface morphologies and as it is possible to investigate a large surface area by the virtue of small angle of incidence. Moreover, GISAXS is the only X-ray technique to elucidate the detailed shape change of the nanostructures both on the surface and inside thin film samples via proper modeling of the scattering data.

II. EXPERIMENTAL

A. Deposition of ZnO: Ge nanocomposite thin film samples

Multilayered thin film samples were deposited on p-type Si (~10 Ω-cm) substrates by sequential sputtering of commercial two-inch ZnO and Ge targets with 99.99% purity.

a)Author to whom correspondence should be addressed. Electronic mail: aceylanabd@yahoo.com. Tel.: +90 312 297 6147. Fax: +90 312 299 3037.

Reuse of AIP Publishing content is subject to the terms at: https://publishing.aip.org/authors/rights-and-permissions. Download to IP: 140.116.200.43 On: Fri, 29 Jul 2016 00:53:55

100 W r.f. and d.c. sputter powers were applied to ZnO and Ge targets, respectively. Prior to loading on a rotating holder, which was at ambient conditions without an intentional heating, Si substrates were dipped into HF:H_2O (1:7) solution for 30 s and rinsed in deionized water for 5 min by ultrasonication so as to remove native oxides. Finally, the substrates were dried with N_2. Before starting thin film deposition, vacuum chamber was pumped down to below 10^{-6} Torr and it was flushed with 500 mTorr Ar three times so as to reduce partial pressures of unwanted gas contents. Five layers of Ge were sequentially stacked between six layers of ZnO. For the reactive sputtering of ZnO layers, 5 mTorr O_2 was introduced to the vacuum chamber in addition to 45 mTorr Ar. For the deposition of Ge layers in both reactive (r) and nonreactive (nr) depositions, 45 mTorr Ar was only employed. In each case, deposition times of ZnO and Ge layers were kept at 10 min and 3 min, respectively. In the case of reactive sputtering, between the ZnO and Ge layer depositions 10 min waiting interval has been utilized to pump out residual O_2. After completing the thin film deposition, samples were exposed to *ex-situ* RTA process so as to initiate Ge-np formation. RTA was carried in a SSI Solaris 75 rapid thermal processor under forming gas (5%H + 95%N_2) atmosphere at 600 °C for 30 s, 60 s, and 90 s.

B. Structural characterization

In our previous works, the detailed structural characterization of ZnO: Ge-nr and ZnO: Ge-r samples performed by various techniques like XRD, SEM, and SIMS has been published elsewhere.[9,10,16] In order to ensure the integrity of this work, crossectional SEM images of 60 s RTA processed nonreactively and reactively grown ZnO: Ge samples are given in Fig. 1. The layered structure of the samples is clearly shown. It should be noted that reactive growth yields more compact structure due to the existence of oxygen ions in the plasma leading to increased kinetic energy of the incident sputtered atoms on the growing film. Therefore, given that the deposition times are the same, reactive growth produces thinner samples compared to nonreactive growth.

C. GISAXS measurements

GISAXS measurements were performed by using a SR beam at beam-line 23 A of the National Synchrotron Radiation Research Center (NSRRC), Taiwan. The analysis of nanosized Ge nanoparticles embedded ZnO is based upon the simultaneous GISAXS. The method was used to determine structural parameters (such as size, shape, and distributions) of nanostructures. Scattering experiments were carried out with the photon energy of 8 keV ($\lambda = 1.54$ Å) and an incidence angle of 0.2°. The pinhole size of S3 & P1 (mm) was 0.50 × 0.50. The GISAXS patterns were recorded by a 2D X-Ray CCD detector (MAR165, 165 mm in diameter, 1024 × 1024-pixel resolution). The entrance window of the detector was perpendicular to the sample surface and to the plane of incidence of the primary radiation and the CCD were situated 312 cm and 515 cm from the samples in order to obtain two different q-range, respectively. The distance between the sample and the detector was 4872.18 mm.

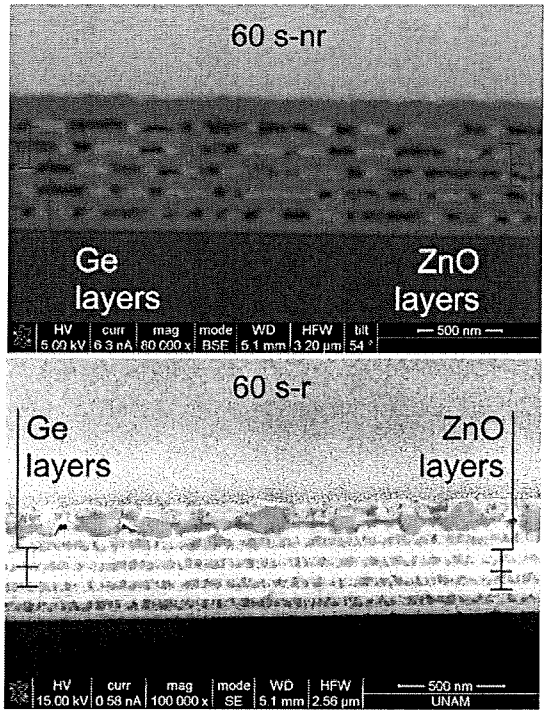

FIG. 1. Crossectional SEM images of nr-ZnO: Ge [top] and r-ZnO: Ge [bottom] thin films RTA processed for 60 s.

III. RESULTS AND DISCUSSION

2D scattering intensity profiles of two sets of ZnO: Ge samples and data collection geometry of GISAXS measurements are shown in Fig. 2. The specular reflection during the

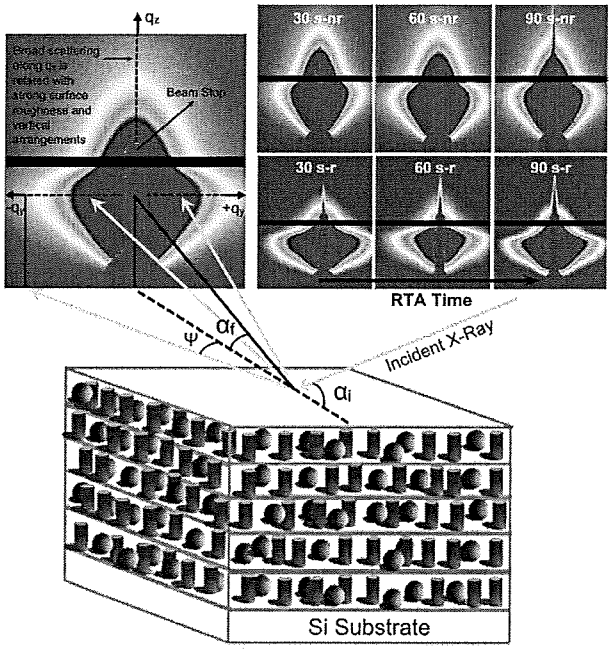

FIG. 2. Schematic drawing of the GISAXS geometry:[21] α_i and α_f are the incident and the exit angle of the X-ray beam, respectively; ψ is the scattering in-plane angle; q_y and q_z are the horizontal and the vertical scattering vectors, respectively; and 2θ is the diffraction angle. Upper right images are the 2D GISAXS intensity profiles of the analyzed samples.

Reuse of AIP Publishing content is subject to the terms at: https://publishing.aip.org/authors/rights-and-permissions. Download to IP: 140.116.200.41 On: Fri, 29 Jul 2016 08:53:55

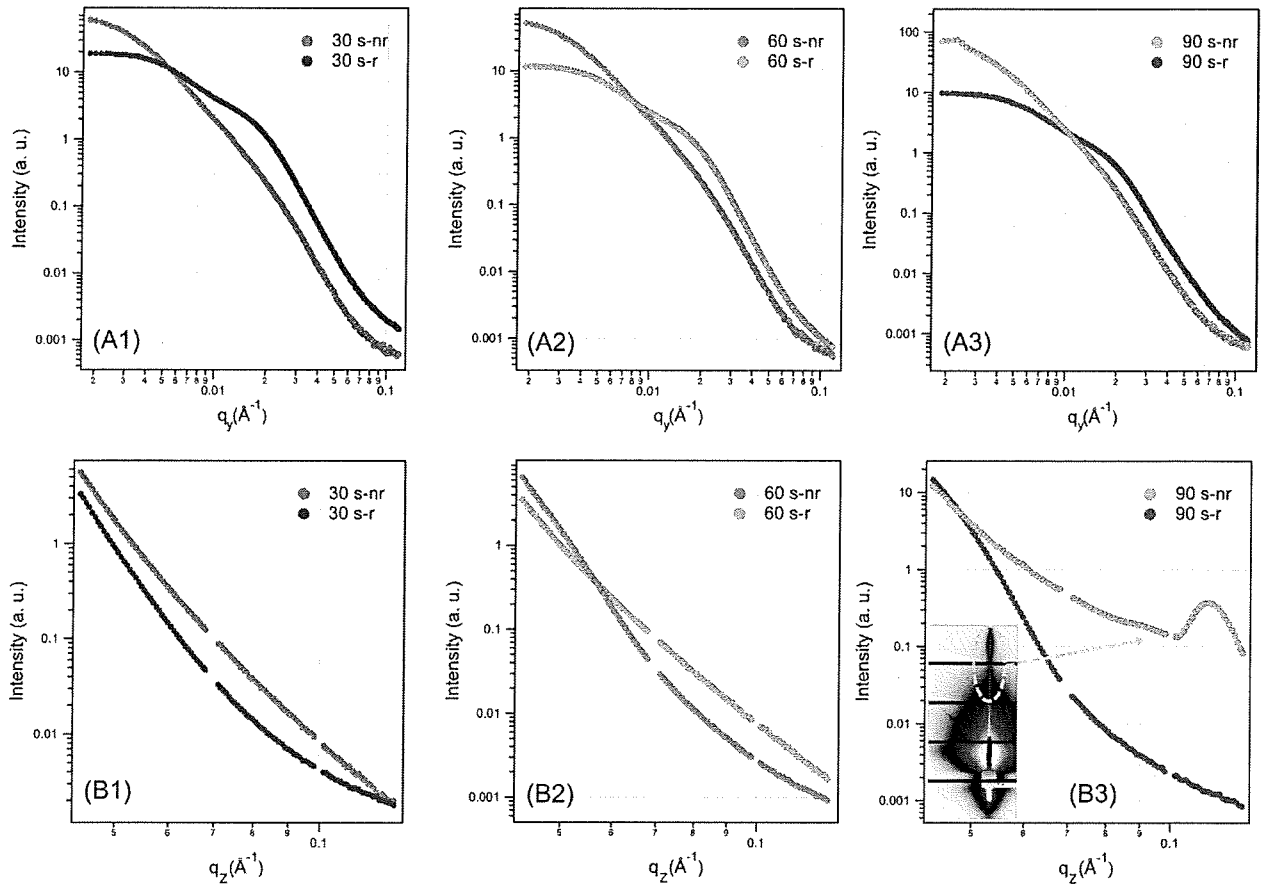

FIG. 3. 1D-GISAXS profiles of the samples along q_y ((A1)–(A3)) and q_z ((B1)–(B3)) directions.

data collection was screened by a beam stop. The color code in the 2D-GISAXS profiles represents different scattering intensities. The scattering vectors q_y and q_z represent two main directions which are horizontal (parallel to the sample plane) and vertical (perpendicular to the sample plane) of the reciprocal space as shown in Fig. 2. The scattering vector q is defined by the wavelength λ, the incidence and exit angles α_i and α_f, and the in-plane scattering angle 2ψ of X-rays as

$$q_y = 2\pi\lambda^{-1}\cos\alpha_f \sin\psi, \quad (1)$$

$$q_z = 2\pi\lambda^{-1}(\sin\alpha_i + \sin\alpha_f). \quad (2)$$

Sharp peaks along q_z seen in 2D GISAXS profiles are evidence of smooth surface and more crystalline arrangements. Therefore, it is readily understood that reactively grown samples acquire not only smooth surface but also better crystallized lattice structure compared to reactively grown samples. Moreover, it is seen that for each sample set q_z peaks get sharper with the increasing RTA time indicating that the structure gets well defined with the application of longer RTA process. In fact, this is in conjunction with the intense diffraction peaks of longer RTA processed samples.

Double logarithmic plots of 1D-GISAXS data taken at critical q-values are shown in Fig. 3. While the plots labelled with **A** belong to q_y direction, **B** labelled ones belong to q_z direction. Although both sample set posses similar scattering patterns along q_y, there is significant difference in q_z plots. This difference notably reveals itself in 90 s RTA processed samples. A nonreactively grown sample acquires a distinct peak. That is indicative of the existence of direction dependent possible crystalline arrangements.

These possible arrangements manifest themselves with the peaks observed from the 1D-GISAXS patterns collected from the directions of 90° (Fig. 3(B3)) and 45° (Fig. 4) with respect to the sample surface. Those peaks are strong evidences of better crystallinity. Therefore, it is understood that RTA process significantly improves the crystallinity of the nonreactively grown samples as compared with the reactively grown ones. This can be attributed to the fact that loose structure of the nonreactively grown samples makes it easier for the better rearrangements of the constituting atoms via self-diffusion mechanisms within a given RTA time.

For the quantitative characterization of the sample structures from the GISAXS data, a cylindrical structure model of Moore's indirect Fourier analyses procedure has been implemented using the IGOR Pro software.[17,18] In Fig. 5, the radial electron density distributions of both sample sets are presented. The plots have been produced by fitting 1D-GISAXS data along q_y. Quantum mechanically delocalized nanoscopic electron density distributions are three-dimensional real space arrangement of the electrons in the material and very informative about surface morphologies.

Reuse of AIP Publishing content is subject to the terms at: https://publishing.aip.org/authors/rights-and-permissions. Download to IP: 140.110.200.41 On: Fri, 29 Jul 2016 08:53:55

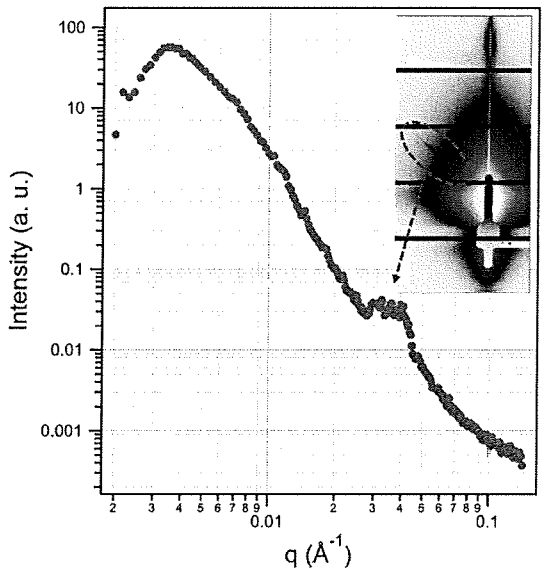

FIG. 4. 45° 1D-GISAXS pattern of nonreactively grown 90 s RTA processed sample. Dashed elliptical line highlights the intensity peak along 45° on 2D-pattern.

Maximum ranges of the nanostructures for nonreactively and reactively grown samples were measured as 800 Å and 400 Å, respectively. Electron density variations of the two sets are also consistent with the fact that reactively grown samples have a compact lattice structure. As for the effect of RTA process on each set, it is noticed that there is an expected trend for the nonreactively grown samples observed from the peak around 500 Å. Not only does it shift to shorter radial distance but also get intense as an indication of better crystalline structure with increasing RTA time. However, reactively grown samples do not follow the similar trend. It is seen that 60 s RTA process results in better crystallinity compared with 90 s. 60 s appears to be the optimum thermal process time for more compact ZnO: Ge structure since longer RTA than necessary might deteriorate the local atomic structure as it is case for the 90 s sample. In fact, careful investigation of 2D-GISAXS profiles of the reactively grown samples along q_y confirms this observation. 60 s RTA processed sample manifests a narrower intensity profile as compared with that of 90 s.

Pair distance distributions (PDD) and particle volume distributions (PVD) of the samples obtained by using a PDDF calculator of NCNR embedded in the Igor Pro software are shown in the left and right panels of Fig. 6, respectively. While PDD plots are produced from the whole $I(q_y)$ data, PVD plots are generated from the middle q-range. PDD plots show that nonreactively grown samples are dominantly composed of *cylindrical* nanostructures whereas reactively grown ones have both *cylindrical* and *spherical* nanostructures. These two formations appear as two distinct peaks. While the left peak corresponds to *spherical*, the right one corresponds to *cylindrical* nanostructures. We attribute these results to better isolation of Ge nanoparticles within the reactively grown ZnO matrix due to the compact structure. Ge nanoparticles form the spherical entities, however, ZnO shapes in c-oriented cylindrical nanostructures as it is usually the case for ZnO thin films. On the other hand, nonexistence of spherical nanostructures in a nonreactively grown ZnO matrix is probably due to loose lattice structure of the embedding layers enabling the lateral clustering of the Ge layers which again fits in cylindrical formation. This is in fact very well consistent with crossectional SEM images of the samples. It is obvious that Ge layers of the nonreactively grown sample cluster as in-plane cylinders. PVD plots also demonstrate a similar result and better distinguish the formation of spherical and cylindrical nanostructures. It is readily realized that spherical nanostructures (i.e., Ge nanoparticles) have a narrow size distribution around 20 nm. This is again in agreement with our previous results. The reactively grown matrix leaves very limited number of vacancies for the RTA induced larger clustering of Ge layers. The compact structure creates local pressure around Ge atoms and forces them to form spherical Ge nanoparticles. Since the size is about the critical limit (i.e., 20 nm), some of the Ge atoms energetically prefer to crystallize in simple tetragonal (known as ST12) lattice whereas the larger ones crystallize in the most common diamond lattice.[16,19]

The quantitative structural parameters extracted from the GISAXS data along q_y by utilizing Moore's indirect Fourier transformation method are given in Table I. It is seen

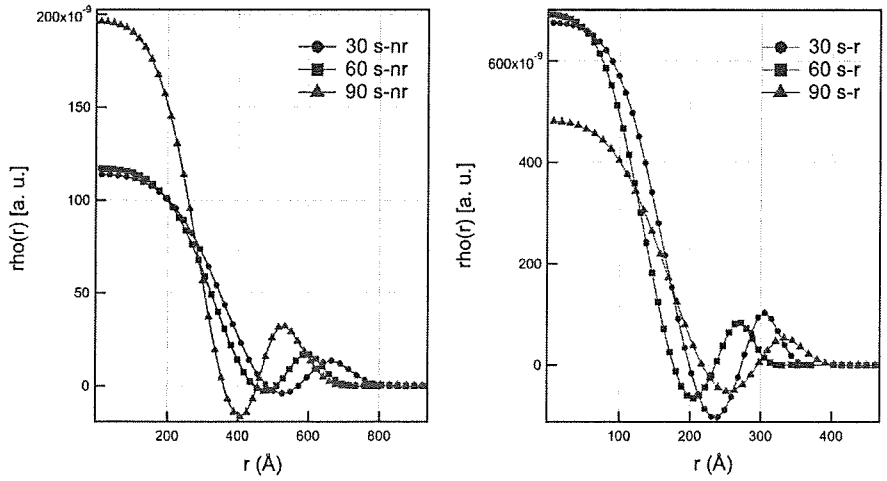

FIG. 5. Radial electron density distributions along the surface for reactively (left) and nonreactively (right) grown ZnO: Ge thin films.

Reuse of AIP Publishing content is subject to the terms at: https://publishing.aip.org/authors/rights-and-permissions. Download to IP: 140.110.200.41 On: Fri, 29 Jul 2016 00:50:55

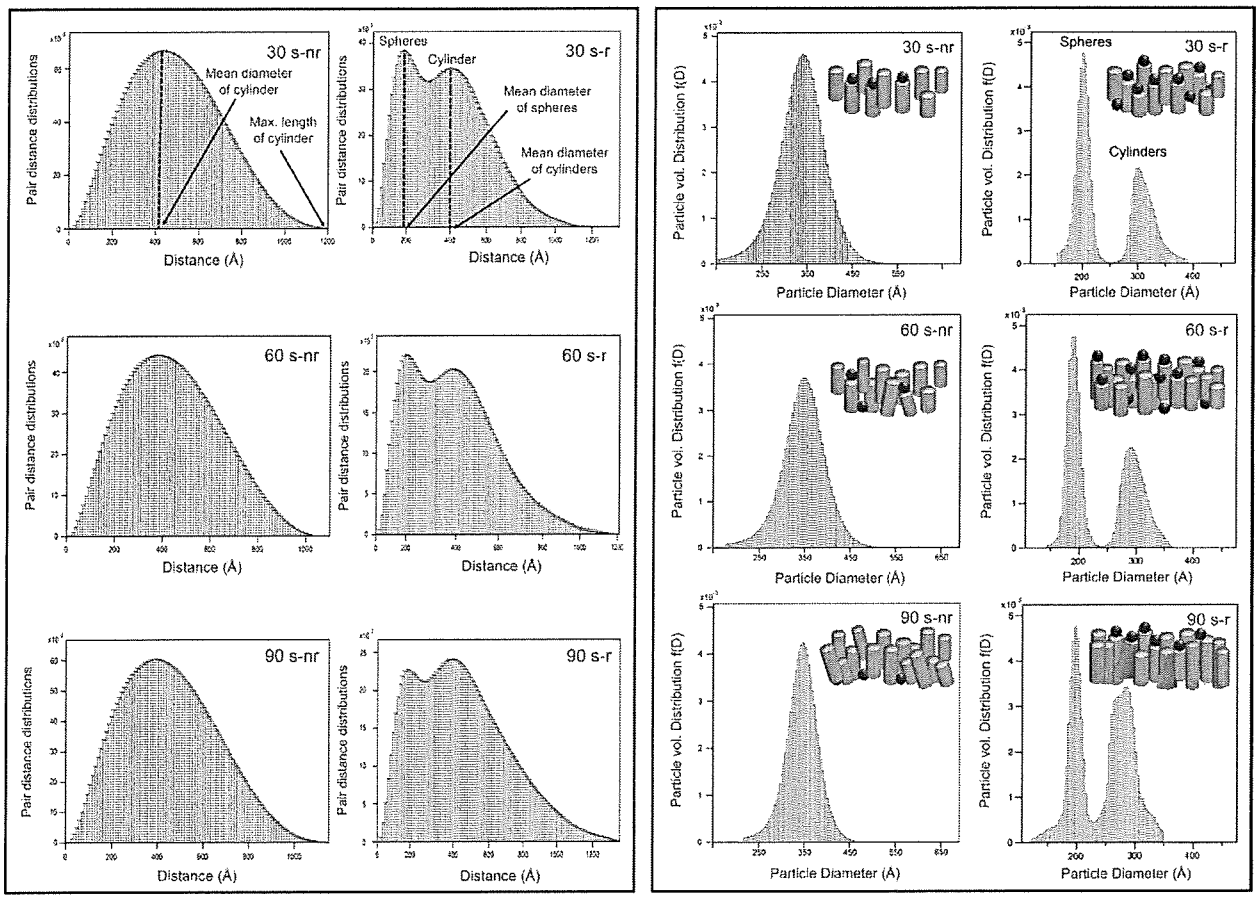

FIG. 6. Pair distance distributions (left) and particle volume distributions (right) of the analyzed nanostructures with respect to particle diameters (χ^2 values for the model fitting process change in the range of 1.9–3.6). The insets in the volume distributions illustrate 3D structural models plotted based on the obtained nanoscopic information and the values are listed in Table I.

TABLE I. The results of GISAXS analyses along q_y and structural parameters of the nanostructures of the samples.

Samples	nr-ZnO			r-ZnO		
Time of RTA process (s)	30	60	90	30	60	90
3D-shape/shapes of the nano aggregations	Cylinder	Cylinder	Cylinder	Cylinder/sphere	Cylinder/sphere	Cylinder/sphere
Mean diameter, ±0.37 (nm)	34.24	35.54	35.01	31.28 and 20.01	29.25 and 17.94	27.53 and 18.85
Max. Length of the cylinders ±0.40 (nm)	120.05	102.83	110.57	109.56	118.24	134.84
Fractal dimension (d_i)	3.98	3.97	4.28	4.60	4.52	4.63
Correlation distance, ±0.56 (nm)	67.62	59.84	52.76	31.88	26.24	33.64

that although RTA time does not significantly affect the mean diameter of the cylindrical nanostructures in the non-reactively grown samples, it gets smaller for the reactively grown samples. On the other hand, spherical nanostructures of the reactively grown samples follow again non-monotonous trend pointing 60 s as the optimum RTA time for reaching smaller Ge nanoparticles. The calculated mean diameter is 17.94 nm, and this is consistent with the crystalline size of ST12 Ge nanoparticles calculated by Scherrer formula.[16] Investigation of the variation of the maximum length of the cylindrical nanostructures in both sample sets reveals that reactive growth enables longer c-axis oriented ZnO formation. This might be attributed to coalescence of ZnO layers in reactively grown samples as opposed to that of nonreactively grown ones.

Fractal dimension, d_i contains information about the surface structure of the samples just as peaks along q_z in 2D-GISAXS profiles. The value of fractal dimension unveils the type of the surface whether it is smooth, mass fractal, or surface fractal.[20] Fractal dimension being close to 4 is known to correspond a smooth surface.

IV. CONCLUSIONS

In this study, the structural evolution of multilayered ZnO: Ge nanocomposite thin films have been investigated

Reuse of AIP Publishing content is subject to the terms at: https://publishing.aip.org/authors/rights-and-permissions. Download to IP: 140.110.200.41 On: Fri, 29 Jul 2016 09:53:56

via the GISAXS technique. The main focus has been to reach a large scale complementary and confirmative information in addition to our previous knowledge about nonreactively and reactively grown ZnO: Ge samples. It has been realized that non-invasive GISAXS measurements do provide additional structural details on the nanostructured thin films as well as supporting the results obtained by other methods like XRD and crossectional SEM. Specifically, the information about the shape and the size distributions of the constituting nanostructures in the ZnO: Ge samples is invaluable. A clear evidence of cylindrical and spherical + cylindrical formations in nonreactively and reactively grown ZnO: Ge samples, respectively, has been gained. Moreover, the structural quantitative data extracted upon data fitting to GISAXS profiles have not only matched very well with the previous information but also provided some extra information.

ACKNOWLEDGMENTS

One of the authors (Professor Semra İde) would like to thank YÖK, NSRRC, and Hacettepe University for the financial grant and the official permissions (respectively) during a scientific research program at NSRRC, Taiwan.

[1]T. Yamamoto and H. Katayama-Yoshida, Jpn. J. Appl. Phys. Lett. **38**, L166 (1999).
[2]M. Arita, M. Yamaguchi, and M. Masuda, Mater. Trans. **45**, 3180 (2004).
[3]M. Jiang, Z. Wang, and Z. Ning, Thin Solid Films **517**, 6717 (2009).
[4]U. Pal and J. G. Serrano, Appl. Surf. Sci. **246**, 23 (2005).
[5]G. H. Shih, C. G. Allen, and B. G. Potter, Jr., Nanotechnology **23**, 075203 (2012).
[6]E. Huttunen-Saarivirta, J. Alloys Compd. **363**, 154 (2004).
[7]D. H. Fan, Z. Y. Ning, and M. F. Jiang, Appl. Surf. Sci. **245**, 414 (2005).
[8]U. Pal, G. C. Segura, and O. Z. Corona, Sol. Energy Mater. Sol. Cells **76**, 305 (2003).
[9]A. Ceylan, A. K. Rumaiz, D. Caliskan, S. Ozcan, E. Ozbay, and J. C. Woicik, J. Appl. Phys. **117**, 105303 (2015).
[10]A. Ceylan, L. Tatar Yildirim, S. Ozcan, and S. Ismat Shah, Mater. Sci. Semicond. Process. **34**, 8 (2015).
[11]C. H. Bates, F. Dachille, and R. Roy, Science **147**, 860 (1965).
[12]J. Joannopoulos and M. Cohen, Phys. Rev. B **7**, 2644 (1973).
[13]P. Liu, Y. L. Cao, X. Y. Chen, and G. W. Yang, Cryst. Growth Des. **9**, 1390 (2009).
[14]S. J. Kim, O. K. Quy, L.-S. Chang, E. A. Stach, C. A. Handwerker, and A. Wei, J. Mater. Chem. **20**, 331 (2010).
[15]J. Liu, C. Liang, Z. Tian, S. Zhang, and G. Shao, Sci. Rep. **3**, 1741 (2013).
[16]A. Ceylan, A. E. Gumrukcu, N. Akin, S. Ozcan, and S. Ozcelik, Mater. Sci. Semicond. Process. **40**, 407 (2015).
[17]S. R. Kline, J. Appl. Crystallogr. **39**, 895 (2006).
[18]D. Babonneau, J. Appl. Crystallogr. **43**, 929 (2010).
[19]Y. Saito, J. Cryst. Growth **47**, 61 (1979).
[20]S. Ayyıldız, E. H. Soylu, S. Ide, S. Kılıç, C. Sipahi, B. Pişkin, and H. S. Gökçe, J. Adv. Prosthodontics **5**, 471 (2013).
[21]M. Lucic Lavcevic, S. Bernstorff, P. Dubček, D. Jozić, I. Jerković, and Z. Marijanović, J. Nanotechnol. **2012**, 1.

Reuse of AIP Publishing content is subject to the terms at: https://publishing.aip.org/authors/rights-and-permissions. Download to IP: 140.110.200.41 On: Fri, 29 Jul 2016 00:52:55